Optical and Quantum Electronics (2023) 55:765
https://doi.org/10.1007/s11082-023-05020-3

Optical mid-infrared modulator based on D-shaped photonic crystal fiber and GST phase changing material

B. M. Younis[1,2] · Nada Yazeed M. Dawood[1,2] · Saleh Mahmoud[1] · Bilal El-Sayed[1] · El-Sayed Usama[1] · Mohamed H. Almoqadem[1] · Mohamed Farhat O. Hameed[2,3,4] · S. S. A. Obayya[2,5]

Received: 28 December 2022 / Accepted: 26 May 2023 / Published online: 28 June 2023

Abstract
Photonic crystal fibers (PCFs) have recently attracted compelling attention because of their numerous applications, particularly in the mid-infrared (mid-IR) wavelength region. In this paper, we have presented and analyzed mid-IR optical modulator based on phase-changing material (PCM) known as germanium-antimony-tellurium (GST) and D-shaped PCF. The modulation process can be performed as the GST material's phase undergoes a transition between amorphous (on) and crystalline (off) states. To analyze the proposed design numerically, full vectorial finite element method (FVFEM) is employed. Further, we studied the light propagation through the suggested structure using 3D finite difference time domain (FDTD) method. The optical losses of the fundamental transverse electric (TE) mode supported by the reported structure in the two GST states are studied. The obtained extinction ratio (ER) of the proposed modulator approaches 302.61 dB, whereas the insertion loss (IL) is less than 0.00014 dB throughout the wavelength range from 3 to 5.8 μm at a device length (L_D) of 0.2 mm. Therefore, the suggested modulator can be utilized in photonic integrated circuits that require high ER, very low IL, and large optical bandwidth.

Keywords Optical modulators · Phase changing materials · GST · Photonic crystal fibers

✉ Mohamed Farhat O. Hameed
mfarahat@zewailcity.edu.eg

✉ S. S. A. Obayya
sobayya@zewailcity.edu.eg

[1] Electronics and Communications Engineering Department, Misr Higher Institute for Engineering and Technology (MET), Mansoura, Egypt

[2] Centre for Photonics and Smart Materials, Zewail City of Science, Technology and Innovation, October Gardens, 6th of October City 12578, Giza, Egypt

[3] Nanotechnology and Nanoelectronics Engineering Program, Zewail City of Science, Technology and Innovation, October Gardens, 6th of October City 12578, Giza, Egypt

[4] Mathematics and Engineering Physics Department, Faculty of Engineering, University of Mansoura, Mansoura 35516, Egypt

[5] Electronics and Communications Engineering Department, Faculty of Engineering, University of Mansoura, Mansoura 35516, Egypt

1 Introduction

Optical modulators (Dawood et al. 2021; Heidari et al. 2021) are essential components in photonic circuits due to their effectiveness in manipulating the light travelling characteristics through photonic/optical circuits/systems. In current photonic integrated circuits (PICs), optical modulators with low transmission loss, immunity to external electromagnetic interference, and large data capacity play a vital role. Due to exceptional light control mechanisms of photonic crystal fibers (PCFs), efficient PCF optical modulators have recently been designed (Dawood et al. 2021; Huang et al. 2019). PCF is a class of optical fiber based on the properties of photonic crystals. They are periodic microstructures based on 2D photonic crystals with air holes usually arranged in hexagonal, square, circular, or rectangular lattice. PCFs (Hameed et al. 2011a; Hameed and Obayya 2009) have been widely used in different applications including biomedical sensors (Azab et al. 2017; Hameed et al. 2016), polarization rotators (Hameed et al. 2011b; Hameed and Obayya 2010) and optical modulators (Dawood et al. 2021; Huang et al. 2019). In this context, Dawood et al. (2021) have proposed a silicon D-shaped PCF-based optical modulator with VO_2 as a phase changing material (PCM) to at $\lambda = 5$ μm. Additionally, a tunable electro-optical modulator based on selectively infiltrated PCF with liquid crystal has been reported in Huang et al. (2019).

Phase changing materials (PCMs) have a growing interest due to their low energy consumption, fast switching speed, and scalability (Cao and Cen 2019). The phase/state of a PCM can be switched by changing the temperature or an external applied electric field (Chen et al. 2015). Germanium-Antimony-Tellurium (GST) is a well-known PCM that has two different phases; the crystalline (off) phase, which exhibits extremely high optical attenuation, and the amorphous (on) phase of a very low light absorption. The phase transition from the amorphous (on) to the crystalline (off) state takes only few nanoseconds and the desired time for the reverse transition is within the range of picoseconds (Wu et al. 2017). The desired time for the phase transition in other PSMs (like VO_2 material) is quite large within the range of milliseconds to nanoseconds (Zhou et al. 2013). Therefore, GST-based devices are faster than those depend on VO_2 as a PCM. In addition, GST-based devices have the advantage of low power consumption due to the non-volatile phase transition of GST and the stability of its state without extra power input (Carrillo et al. 2016). The phase of GST can be controlled via the Joule-heating mechanism by applying a proper voltage between two electrical contacts (Shadmani and Miri 2019). In order to switch the state of GST from amorphous (on) to crystalline (off), it should be heated to a temperature between its crystallization point and melting point, i.e.: $413°K < T < 891°K$. On the other hand, the crystalline (off) to amorphous (on) GST phase transition is induced by heating to a temperature above its melting point ($T > 891°K$) (Shadmani and Miri 2019). The GST has been used in nanophotonic structures to provide efficient devices such as optical modulators (Shadmani et al. 2019; Shadmani and Miri 2019), tunable and switchable plasmonic perfect absorbers (Tian et al. 2020).

The mid-infrared (mid-IR) wavelength range is crucial for both research and industry (Lavchiev and Jakoby 2016). Additionally, Optical communication systems with ultra-compact and high-speed photonic integrated circuits (PICs) based optical devices are in great demand. Therefore, the development of high-speed optical modulators would also have a great impact on free space optics (FSO) communication applications in the mid-infrared range that contains two atmospheric transparency windows (i.e., 3–5 and 8–14 μm) (Luzhansky et al. 2015; Montesinos-Ballester et al. 2022; Su et al. 2018). Thus,

the proposed optical modulator fits the first atmospheric transparency window in FSO. In addition, many optical devices have been reported in literature (Hossain et al. 2021; Hui et al. 2018; Sadeghi et al. 2020; Zheng 2021) to work in the same wavelength range (3–5.8 μm). Due to silicon's low loss in the mid-IR regime (Soref 2010), it has a growing interest in optical communication systems, that enables photonic circuits to migrate to mid-IR wavelength regime. Further, carrier control in silicon allows for a variety of useful applications, including optical modulators (Yamada et al. 2014). Liu et al. (2004) have proposed a high-speed silicon optical modulator based on a metal–oxide–semiconductor capacitor. Additionally, in the mid-IR regime (8–14 μm), an effective acousto-optical light modulation has been developed in Sopko et al. (2020). In this context, a dual polarization GST-on-silicon nitride optical modulator has been presented with an IL of 1.15 dB and ER of 8.12 dB for the TE mode (Shadmani and Miri 2019). However, the IL, and ER are 0.57 dB and 1.75 dB, respectively for the TM mode (Shadmani and Miri 2019). Additionally, Shadmani et al. (2019) have proposed an ultra-wideband multi-level optical modulator based on GST with low power consumption and small footprint with IL of 1.9 dB. Further, Jeyaselvan et al. (2020) have designed an optical modulator using microstrip heater with a VO_2 patch that achieved an IL below 1.4 dB and an ER of 1.4 dB.

In this paper, an efficient optical modulator is designed and analyzed based on silicon D-shaped PCF and GST (GST-D-PCF) as a PCM. The background material of the GST-D-PCF is silicon. The air holes of the silicon GST-D-PCF are arranged in hexagonal lattice. The GST material in the reported GST-D-PCF modulator is used to modulate the input signal. The modulator has a very low IL in its ON state when GST is in the amorphous (on) phase. However, the modulator will be in the OFF state with high loss because of the GST material's phase transition into the crystalline (off) phase. Full vectorial finite element method (FVFEM) (Rajarajan et al. 2000) is employed to calculate the characteristics of the supported modes through the PCF structure i.e., loss and effective index (n_{eff}). Additionally, the 3D finite difference time domain (3D-FDTD) method (Oskooi et al. 2010) is employed to study the light propagation throughout the longitudinal direction. Further, the geometrical parameters of the reported GST-D-PCF modulator are optimized throughout the whole wavelength regime from 3 to 5.8 μm to achieve an extremely high ER of 1547 dB/mm and ultra-low IL that is less than 0.002 dB/mm. The obtained modulator has high ER and comparable IL to those previously reported in the literature (Dawood et al. 2021; Jeyaselvan et al. 2020; Shadmani et al. 2019; Shadmani and Miri 2019).

2 Design considerations

Figure 1 depicts the 2D cross sectional of the GST-D-PCF optical modulator and 3D views. The suggested PCF has a hexagonal arrangement of five air holes rings in a background of Silicon (Si) material that is optically transparent at high levels in the mid-IR region (Zhang et al. 2014). The air holes have a diameter of $d = 0.8\Lambda$ where Λ is the distance between the centers of two adjacent air holes and it is fixed to 2.3 μm as depicted in Fig. 1. The distance between the polished surface of the D-shaped PCF and the upper surface of the air holes (h) equals 150 nm. To obtain the process of modulation, a thin layer of GST material with a thickness t_g of 70 nm is deposited on top of a thin calcium fluoride (CaF_2) with thickness $t_c = 10$ nm as a spacer. Calcium fluoride (CaF_2) material has a wide transparency window that spans from $\lambda = 0.15$ μm to $\lambda = 9$ μm (Doualan et al. 2007; Liu et al. 2014) as well as it provides higher index contrast when utilized

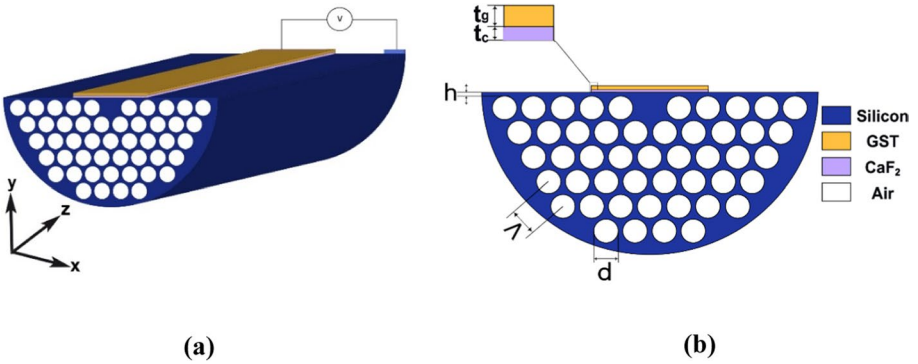

Fig. 1 (**a**) 3D, and (**b**) 2D Cross sectional views of the reported GST-D-PCF optical modulator with a GST layer deposited above CaF_2 spacer

with silicon based waveguides. Thus, CaF_2 appears a suitable substrate material for many devices in the mid-infrared region including polarization splitters (Kumari et al. 2019; Wang et al. 2022), polarization rotators (Kumari et al. 2018; Wang et al. 2021), optical absorbers (Bakan et al. 2018; Peng et al. 2020), and optical modulators (Alrayk et al. 2021). In addition, silicon-on-CaF_2 platform is common in different applications in the mid-infrared wavelength regime as reported in Alrayk et al. (2021), Businaro et al. (2012) and Chi et al. (2019). In the proposed D-PCF structure, a thin CaF_2 layer is deposited on the polished surface of the D-shaped PCF as a spacer to isolate the silicon core from the GST layer. Regarding the fabrication process, it is easy to deposit the CaF_2 layer on silicon which has been extensively implemented in the literature (Wen et al. 2020).The GST and CaF_2 layers have the same width of 5d where d is the diameter of the air holes. Moreover, the GST layer is deposited on the PCF's polished surface near the core region to simplify the interaction with the incoming light. Consequently, the process of modulation is improved. The refractive index (n) and extinction coefficient (κ) of the GST material through the considered wavelength range from 3 to 5.8 μm are reported in (Vassalini et al. 2021). It is worth mentioning that there is a significant difference (~2) in the real part of the refractive index (n) of the GST material between the crystalline and amorphous states. However, the extinction coefficient (κ) in the amorphous GST state is very small (~zero). On the other hand, in the crystalline GST phase, κ is larger and generally increases by increasing the wavelength. For example, at $\lambda = 3$ μm, κ is approximately zero in GST amorphous state, whereas in the crystalline GST state, κ is ~0.5. This reveals the high absorption that occurs in the crystalline GST state when compared to that in the amorphous GST state. At $\lambda = 3$ μm, n in the amorphous GST state is ~4, and in the crystalline GST state is ~6. These large differences in n and κ between the two GST phases are exploited to induce the required modulation behavior. Through the whole wavelength range from 3 to 5.8 μm, n is approximately constant and equal to 4, while in a crystalline state, n is slightly varying around a value of 6. However, κ in the amorphous state is nearly constant (~zero) in the studied wavelength range from 3 to 5.8 μm, but in the crystalline state, κ generally increases by increasing wavelength.

The Sellmeier equation calculates the Si material dispersion in the mid-IR region as in Chandler-Horowitz and Amirtharaj (2005):

$$n^2(\lambda) = 11.67316 + \frac{1}{\lambda^2} + \frac{0.004482633}{\lambda^2 - 1.108205^2} \quad (1)$$

where λ is the wavelength in microns. In addition, the wavelength-dependent Sellmeier equation utilized to determine CaF_2's refractive index is reported in Malitson (1963):

$$n^2(\lambda) = \frac{0.5675888\lambda^2}{\lambda^2 - 0.050263605^2} + \frac{0.4710914\lambda^2}{\lambda^2 - 0.1003909^2} + \frac{3.8484723\lambda^2}{\lambda^2 - 34.649040^2} + 1 \quad (2)$$

To obtain high ER optical modulator, the optical loss in the ON state (amorphous GST phase) or IL should be minimized, while the optical loss in the OFF state (crystalline GST phase) should be maximized. The geometrical parameters of the proposed design, such as GST thickness (t_g), CaF_2 thickness (t_c), the distance between the air holes' upper surface and the polished surface (h), the hole pitch (Λ), and air holes' diameter (d) depicted in Fig. 1(b) are studied separately to optimize the IL and ER of the proposed design.

PCF fabrication and drawing technology has become extremely mature. Then, D-shaped PCFs can be fabricated by side polishing the conventional PCF (Xie et al. 2017). Furthermore, the side polished length can be controlled accurately as proposed in Xie et al. (2017), which can meet the requirements of different designs. For the GST deposition process, both physical vapor deposition (PVD) and chemical vapor deposition (CVD) can be applied (Suda et al. 2013). The phase of the GST layer can be controlled through the Joule-heating mechanism and by applying a proper voltage pulse to the electrical contacts (Shadmani and Miri 2019) as shown in Fig. 1(a). In light of this, the CaF_2 layer below the GST layer can be created using an ion milling transfer of photoresist lenses which is fabricated by three different techniques; a melting resist technique (Flamm et al. 2000), a gray scale lithography (Flamm et al. 2000) and hot-pressing technique (Zhou et al. 2014). Accordingly, the suggested GST-D-PCF optical modulator can be fabricated using the current technologies (Lyeo et al. 2006).

3 Results and discussion

The study and analysis of the suggested GST-D-PCF modulator are performed using FVFEM (Obayya et al. 2002) via COMSOL Multiphysics software package (https://www.comsol.com). The fundamental mode characteristics i.e., optical loss and effective index (n_{eff}) of the supported modes are analyzed. It is worth mentioning that the simulation domain is truncated from all transverse directions by a perfectly matched layer (PML) (Koshiba and Tsuji 2000) as an absorbing boundary condition. The reported structure is divided into tiny triangular elements with non-uniform meshing capabilities. In addition, extensive convergence tests are performed for the proposed structure to make sure that the results are stable and numerically accurate. According to the numerical results, the convergence occurs when the thickness of PML is larger than 0.3 μm with a maximum mesh element size that is less than 3.0 μm. To ensure stable performance, a 1.0 m thick PML and a maximum mesh element size of 0.5 μm are employed. Additionally, to guarantee enough mesh in GST and CaF_2 thin layers, a minimum mesh element size of 2 nm is applied.

The field distributions of the transverse electric (TE) and transverse magnetic (TM) modes supported by the core region of the GST-D-PCF, are shown in Fig. 2. The initial geometrical parameters utilized to perform this study are depicted in Table 1. As shown in Fig. 2(a), the fundamental TM core mode is sufficiently confined in the PCF core and has

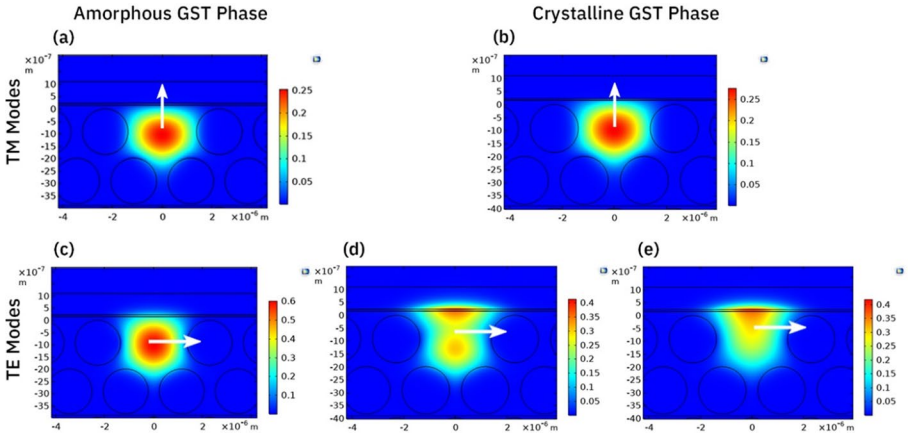

Fig. 2 The field distributions of the (**a**) TM core mode for at amorphous (on) GST phase, (**b**) TM core mode at the crystalline (off) GST phase, (**c**) TE core mode at the amorphous (on) GST phase, (**d**) TE core mode at the crystalline (off) GST phase, and (**e**) SPM at the crystalline (off) GST phase. The utilized geometrical parameters in this study are depicted in Table 1

Table 1 The reported structure's initial geometrical parameters

Parameter	t_g	t_c	H	D	Λ	L_D
Value	70 nm	10 nm	150 nm	0.8Λ	2.3 μm	0.1 mm

a very low optical loss. By switching the phase of GST material, thanks to the externally applied voltage, from amorphous (on) to crystalline (off), the optical loss of the fundamental TM mode is not significantly affected, as shown in Fig. 2(b). On the other hand, the TE mode suffers high optical absorption at the same GST phase, as depicted in Fig. 2(c) and (d). As may be seen in Fig. 2(c), the TE mode is well confined with low optical loss in the amorphous (on) phase. Though, in the crystalline (off) phase, Fig. 2(e), the plasmonic behavior of the GST material in this case causes the TE core mode to be attracted toward the GST layer with a significant optical loss. The reason behind that is the phase matching between the TE core mode (Fig. 2(d)) and a TE surface plasmon modes (SPMs) constructed on the surface of the crystalline (off) GST layer, Fig. 2(e). Accordingly, the energy of the TE core mode is transferred to the SPM with high loss. Figure 3 depicts the dispersion spectra of the TE core mode and the SPM. As shown in Fig. 3, there is a strong coupling between the core mode and the SPM which leading to a distinct loss peak at $\lambda = 3.9$ μm. At this wavelength, the effective indices of the TE core mode and SPM are equal, Fig. 3. Therefore, the TE mode effectively achieves the modulation behavior.

Figure 4(a) shows the calculated optical loss of both TE and TM core modes in OFF State (crystalline GST) and ON State (amorphous GST) through 3–5.8 μm wavelength range. It is worth noting that the extinction coefficient (κ) of crystalline (off) GST is extremely high ($\kappa = 0.7157$ at $\lambda = 3.9$ μm) while it is very low when GST is in its amorphous (on) phase. As may be seen from Fig. 4(a), in OFF state (crystalline GST), the propagation loss of the TE mode is remarkably greater than the TM mode. This is because the TE core mode and the SPM are strongly coupled. Additionally, the phase matching between the TE mode and SPM occurs at $\lambda = 3.9$ μm with an optical loss of 1025 dB/mm. In the ON state (amorphous GST), the optical loss of the TE mode is slightly higher than

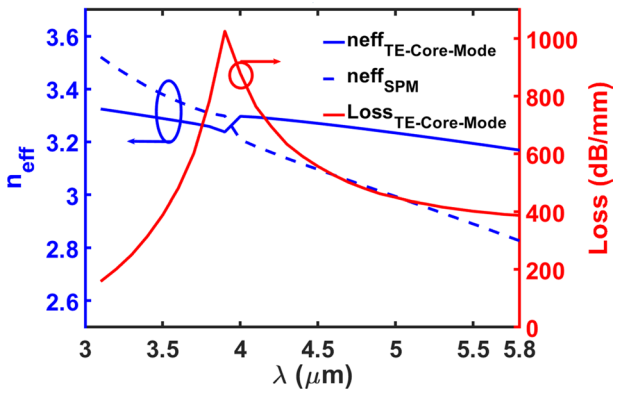

Fig. 3 Dispersion and loss spectra of the TE core-guided mode and SPM mode. The utilized geometrical parameters in this study are depicted in Table 1

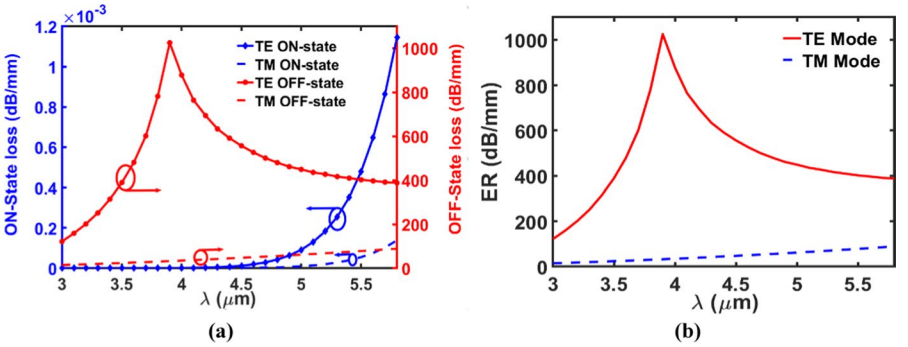

Fig. 4 **(a)** The optical loss spectra of the TE and TM core modes in the OFF and ON states; dashed lines denote the TM mode, and solid lines represent the TE mode, and **(b)** the calculated wavelength dependent ER of the fundamental TE and TM core modes. The utilized geometrical parameters in this study are depicted in Table 1

that of the TM mode, Fig. 4(a). It may be seen from Fig. 4(b) that the TE mode has higher ER than that of the TM mode. In optical modulators, it is required to maintain a very low loss at the ON State (minimize IL) while suppressing the operating mode at the OFF State. This will increase ER ($Loss^{OFF-state}$–$Loss^{ON-state}$). Thus, our main objective is to demonstrate that the TE mode is completely suppressed in the OFF State, regardless of the value of the loss.

The 3D-FDTD simulations via Lumerical software package (https://www.lumerical.com) are then performed to investigate the propagation properties of both TE and TM modes of the reported GST-D-PCF structure. The reported modulator is supposed to have an initial device length of 50 μm. In this study, the simulation domain is discretized with Δx, Δy, and Δz of 0.09 μm, 0.01 μm, and 0.6 μm, respectively while PML boundary conditions are applied to all transverse directions. In Fig. 5, the field evolution along the proposed structure's longitudinal direction is shown at amorphous (on) and crystalline (off) phases of GST at λ = 3.9 μm. As may be seen in Fig. 5(a) and (c), the propagation loss of both TE and TM cores modes is very low throughout the device length when the GST material is in its amorphous (on) phase. Additionally, the TM core mode is slightly affected by the phase transition of GST material and still exhibits small propagation loss through

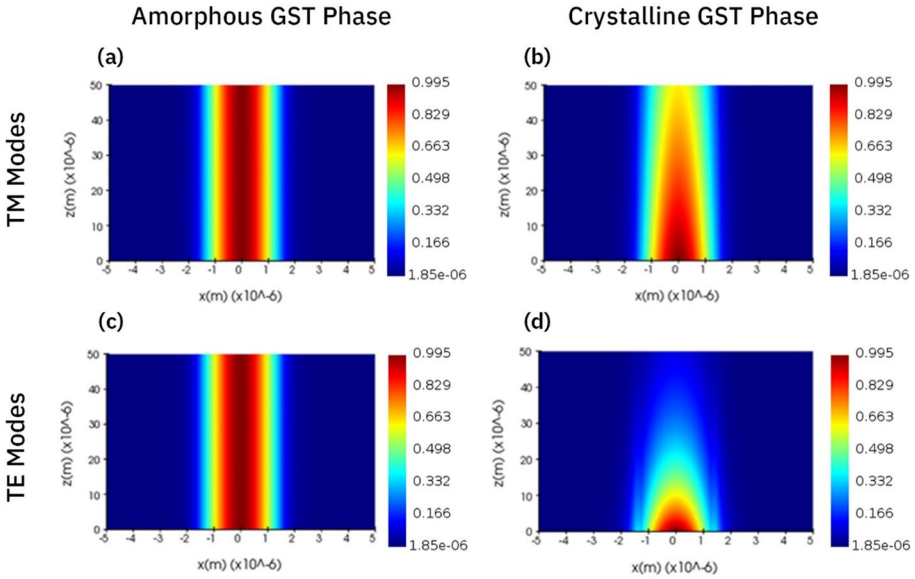

Fig. 5 Light propagation of the (**a**) TM mode at amorphous (on) GST phase, (**b**) TM mode at crystalline (off) GST phase, (**c**) TE mode at amorphous (on) GST phase, and (**d**) TE mode at crystalline (off) GST phase at $\lambda = 3.9\,\mu m$. The utilized geometrical parameters in this study are depicted in Table 1

the modulator length, Fig. 5(b). On the other hand, in crystalline (off) GST phase, the TE core mode is greatly absorbed by the lossy GST layer due to strong coupling with the SPM, as shown in Fig. 5(d). As a result, only the TE mode is considered in the subsequent studies in this work.

To investigate the impact of different geometrical parameters on the implementation of the suggested modulator, a separate analysis to the effect of each geometrical parameter on the ER and IL is executed. In each study, one parameter is studied where all other geometrical parameters are kept to their initial values summarized in Table 1. First, the effect of GST thickness (t_g) is investigated. Figure 6(a) and (b) show the wavelength dependent ER and IL of the suggested modulator, respectively at various GST thicknesses. Figure 6(a) shows that by increasing t_g, the ER slightly increases. However, the resonance peak position of ER is shifted from $\lambda = 3.4$ μm at $t_g = 60$ nm to $\lambda = 5.4$ μm at $t_g = 100$ nm. This shift is due to the fact that the phase-matching between the core mode and SPM is a wavelength sensitive process. When the GST thickness is changed, the SPM optical characteristics changes and the phase matching wavelength accordingly changes. As may be seen in Fig. 6(b), by increasing t_g through wavelengths between 3 and 5.8 μm, IL slightly increases. While in all studied GST thicknesses, the IL is still lower than 0.0015 dB/mm through the whole wavelength range. However, the maximum value of IL is less than 0.002 dB/mm as the extinction coefficient of GST in amorphous (on) phase is very low. As a result, t_g is set to 100 nm to sustain the balance between the ER and IL of the reported modulator. At $t_g = 100$ nm, the ER is 1186 dB/mm while an IL below 0.002 dB/mm is obtained at $\lambda = 5.5$ μm.

The Si core and GST layer are effectively separated by the low index CaF_2 layer. Thus, CaF_2 dielectric spacer plays a pivotal role in controlling the performance of the presented modulator. Accordingly, the effect of CaF_2 layer thickness (t_c) on the ER and IL is studied

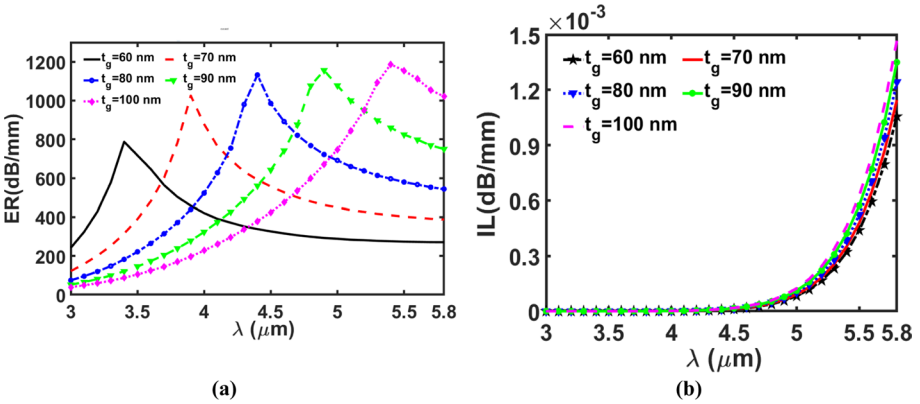

Fig. 6 Wavelength dependent (**a**) ER and (**b**) IL of the suggested GST-D-PCF modulator at different t_g values while all other geometrical parameters are kept at their initial values summarized in Table 1

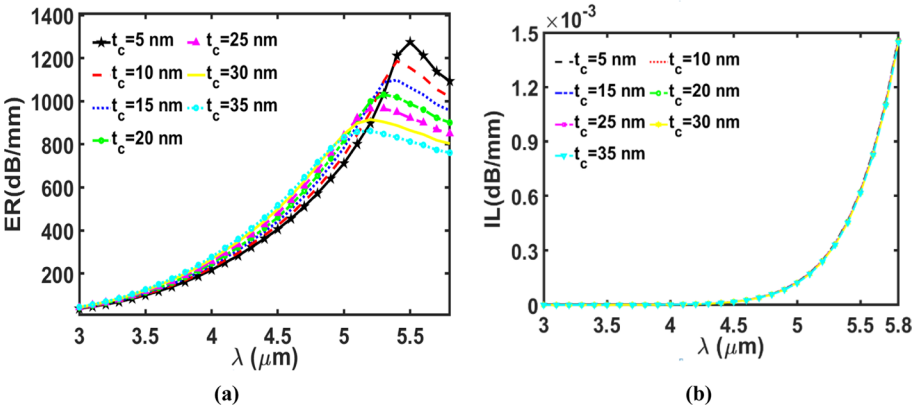

Fig. 7 Wavelength dependent (**a**) ER and (**b**) IL of the suggested GST-D-PCF modulator at different t_c values. All other geometrical parameters are kept at their initial values summarized in Table 1 while tg is fixed to 100 nm

in detail. All geometrical parameters in this study are maintained at their initially set values summarized in Table 1 except t_g that is set to 100 nm. Figure 7(a) and (b) illustrate the ER and IL as a function of the wavelength at different values of t_c. As may be seen in Fig. 7(a), the resonance peak position of ER is shifted to longer wavelengths by decreasing t_c. Further, by increasing t_c, the IL does not change as shown in Fig. 7(b). At longer wavelengths, a trade-off occurs between the IL and ER as the increase in ER is accompanied with the increase in IL. However, the maximum value of IL is still less than 0.002 dB/mm. Therefore, t_c is fixed to 5 nm, where the ER and IL are equal to 1274 dB/mm and 0.002 dB/mm, respectively at $\lambda = 5.5$ μm.

It is also important to investigate how the reported modulator behaves in regard to the change in PCF filling factor (d/Λ). In this investigation, t_g and t_c are set to 100 and 5 nm, respectively while all other geometrical parameters are fixed to their initial values depicted in Table 1. Figure 8 shows the wavelength dependent ER and IL at different values of d/Λ

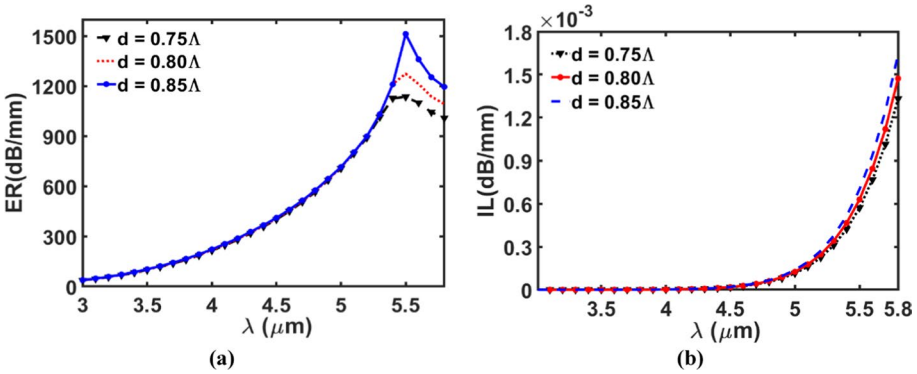

Fig. 8 Wavelength dependent (**a**) ER and (**b**) IL of the suggested GST-D-PCF modulator at different values of PCF filling factor. All other geometrical parameters are kept at their initial values summarized in Table 1 while tg and t_c are set to 100 and 5 nm, respectively

throughout the wavelength regime from 3 to 5.8 μm. As shown in Fig. 8(a) and (b), by increasing d/Λ, the ER and IL increase while the maximum value of IL is still less than 0.002 dB/mm. To have the highest allowable ER and keep IL at small values, d/Λ = 0.85 is chosen. At this value, the calculated ER and IL of the proposed modulator are 1513 dB/mm and 0.002 dB/mm, respectively at λ = 5.5 μm.

Figure 9 depicts the ER and IL spectra at different h values. It is important to note that, as shown in Fig. 1, h is the distance between the polished surface and the upper surface of the air holes. It could be noted that as h increases, the GST layer places far from the core region, which reduces the core field's absorption. As depicted in Fig. 9(a) and (b), ER decreases and IL is approximately fixed as h is increased over the studied wavelength range. However, the fabrication process will get more difficult if h is reduced to 100 nm or below. To have the highest allowable ER and keep IL at small values and to ensure the ease of fabrication, h = 150 nm is chosen. At h = 150 nm, the calculated ER and IL values are 1513 dB/mm and 0.00069 dB/mm, respectively at λ = 5.5 μm.

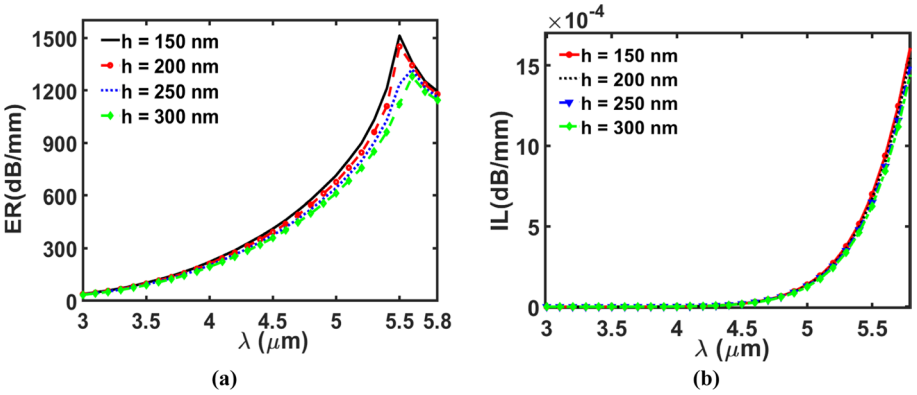

Fig. 9 Wavelength dependent (**a**) ER and (**b**) IL of the suggested GST-D-PCF modulator at different values of PCF filling factor. All other geometrical parameters are kept at their initial values summarized in Table 1 while t_g, t_c and d/Λ are set to 100, 5 nm, and 0.85, respectively

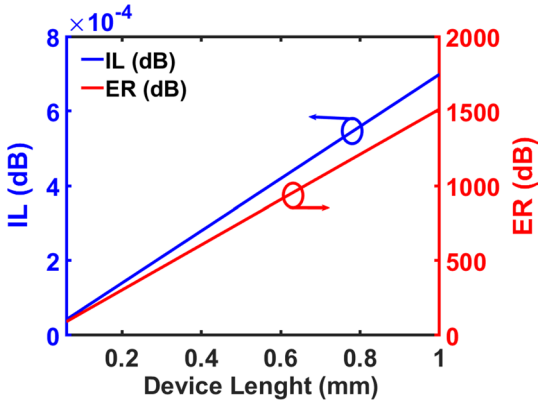

Fig. 10 Variation of ER and IL with the device length at the optimized geometrical parameters and at $\lambda = 5.5$ μm

Using the FDTD method (Oskooi et al. 2010) via Lumerical software package (https://www.lumerical.com), the TE core mode propagation through the modulator structure is investigated as a function of device length (L_D) at $\lambda = 5.5$ μm. The calculated ER and IL as a function of L_D are depicted in Fig. 10. The optimized geometrical parameters $t_g = 100$ nm, $t_c = 5$ nm, $h = 150$ nm, $d = 0.85$, and $\Lambda = 2.3$ m are used in this study. The results in Fig. 10 indicate that ER increases by increasing L_D where it reaches 1513 dB at $L_D = 1$ mm. Additionally, the obtained IL of the proposed modulator is in the order of 10^{-6} with slight changes according to the change in L_D. Therefore, to keep ER at high levels and keep the compactness of the reported modulator, L_D is set to 0.2 mm with an ER and IL of 302.61 dB and 0.00014 dB, respectively at $\lambda = 5.5$ μm.

In order to show the significance of the presented modulator, it is compared to those previously reported in the literature in terms of the main platform, the active material employed, operating wavelength, ER, and IL. When compared to the results reported in (Dawood et al. 2021; Fu et al. 2020; Jeyaselvan et al. 2020; Sadeghi et al. 2020; Shadmani et al. 2019), the suggested GST-D-PCF modulator has a high ER with very small IL as depicted in Table 2. It is worth mentioning that the reported modulator has a comparable ER and much smaller IL than that reported in (Dawood et al. 2021) based on the same platform but with VO_2 as a PCM. However, GST material has faster switching speed than VO_2 (Cao and Cen 2019).

4 Conclusion

An optical modulator based on D-shaped PCF and GST material as a PCM is numerically analyzed via FVFEM and 3D FDTD. The reported D-shaped PCF is composed of a silicon background material and a GST layer that is deposited on top of a CaF_2 spacer to get the modulation behavior. By electrically switching the phase of GST material from amorphous (on) to crystalline (off), the TE mode can be significantly suppressed by means of strong coupling with the SPM constructed on the GST layer's surface. Thus, the modulated signal is obtained. With a device length of 0.2 mm, the simulation results reveal that throughout the mid-IR wavelength regime of 3 to 5.8 μm, the reported modulator provides an ultrahigh ER of 302.61 dB and very low IL of less than 0.00014 dB. In comparison to other PCF

Table 2 Compares the proposed device modulating performance to those reported in the literature (Dawood et al. 2021; Fu et al. 2020; Jeyaselvan et al. 2020; Sadeghi et al. 2020; Shadmani et al. 2019)

Device	Experiment/modelling	Platform	Active material	L_D (μm)	λ (μm)	ER (dB)	IL (dB)
Shadmani and Miri (2019)	FEM and 3D-FDTD modelling	Waveguide	GST	4	1.2–1.7	8.12	1.15
Jeyaselvan et al. (2020)	Experimental	SOI	VO_2	–	~1.55	25	1.4
Fu et al. (2020)	FEM modelling	PCF	Graphene	205	1.25–1.9	7	–
Sadeghi et al. (2020)	3D-FDTD modelling	SOI	VO_2	1	3.8	4.4	0.1
Dawood et al. (2021)	FEM and 3D-FDTD modelling	D-PCF	VO_2	500	3.0–7.0	~236	< 1.3
Proposed modulator	FEM and 3D-FDTD modelling	D-PCF	GST	200	3.0–5.8	~302.61	0.00014

based modulators that were previously reported in the literature, the suggested modulator achieves a very low IL, high ER, and large bandwidth with a compact L_D.

Author contributions BMY, MFOH, and SSAO have proposed the idea. SM, BE-S, E-SU, MHA and NYMD have performed the simulations of the reported modulator. All authors have contributed to the analysis, discussion, writing and revision of the paper.

Funding Open access funding provided by The Science, Technology & Innovation Funding Authority (STDF) in cooperation with The Egyptian Knowledge Bank (EKB). No fund is associated with the current manuscript.

Availability of data and materials The data will be available upon request.

Declarations

Competing interests The authors would like to clarify that there are no financial/non-financial interests that are directly or indirectly related to the work submitted for publication.

Ethical approval The authors declare that there are no conflicts of interest related to this article.

References

Alrayk, Y.K.A., Younis, B.M., El Deeb, W.S., Hameed, M.F.O., Obayya, S.S.A.: MIR optical modulator based on silicon-on-calcium fluoride platform with VO_2 material. Opt. Quantum Electron. **53**, 1–16 (2021)

Azab, M.Y., Hameed, M.F., Obayya, S.S.A.: Multi-functional optical sensor based on plasmonic photonic liquid crystal fibers. Opt. Quantum Electron. **49**, 1–17 (2017)

Bakan, G., Ayas, S., Dana, A.: Tunable enhanced infrared absorption spectroscopy surfaces based on thin VO_2 films. Opt. Mater. Express. **8**, 2190–2196 (2018)

Businaro, L., Limaj, O., Giliberti, V., Ortolani, M., Di Gaspare, A., Grenci, G., Ciasca, G., Gerardino, A., De Ninno, A., Lupi, S.: Mid-infrared nanoantenna arrays on silicon and CaF_2 substrates for sensing applications. Microelectron. Eng. **97**, 197–200 (2012)

Cao, T., Cen, M.: Fundamentals and applications of chalcogenide phase-change material photonics. Adv. Theory Simul. **2**, 1900094 (2019)

Carrillo, S.G.-C., Nash, G.R., Hayat, H., Cryan, M.J., Klemm, M., Bhaskaran, H., Wright, C.D.: Design of practicable phase-change metadevices for near-infrared absorber and modulator applications. Opt. Express **24**, 13563–13573 (2016)

Chandler-Horowitz, D., Amirtharaj, P.M.: High-accuracy, midinfrared ($450\ cm^{-1} \leqslant \omega \leqslant 4000\ cm^{-1}$) refractive index values of silicon. J. Appl. Phys. **97**, 123526 (2005)

Chen, Y., Li, X., Luo, X., Maier, S.A., Hong, M.: Tunable near-infrared plasmonic perfect absorber based on phase-change materials. Photonics Res. **3**, 54–57 (2015)

Chi, J., Liu, H., Huang, N., Wang, Z.: A broadband enhanced plasmonic modulator based on double-layer graphene at mid-infrared wavelength. J. Phys. D Appl. Phys. **52**, 445101 (2019)

COMSOL 5.1 Multiphysics software. https://www.comsol.com

Dawood, N.Y.M., Younis, B.M., Areed, N.F.F., Hameed, M.F.O., Obayya, S.S.A.: Mid-infrared optical modulator based on silicon D-shaped photonic crystal fiber with VO_2 material. Appl. Opt. **60**, 9488–9496 (2021)

Doualan, J.L., Camy, P., Moncorgé, R., Daran, E., Couchaud, M., Ferrand, B.: Latest developments of bulk crystals and thin films of rare-earth doped CaF_2 for laser applications. J. Fluor. Chem. **128**, 459–464 (2007)

Flamm, D., Schindler, A., Harzendorf, T., Kley, E.-B.: Fabrication of microlens arrays in CaF_2 by ion milling. In: Lee, S.H., Johnson, E.G. (eds.) Micromachining Technology for Micro-optics, pp. 108–116. International Society for Optics and Photonics, Santa Clara (2000)

Fu, G., Wang, Y., Wang, B., Yang, K., Wang, X., Fu, X., Jin, W., Bi, W.: A compact electro-absorption modulator based on graphene photonic crystal fiber. Chin. Phys. B **29**, 34209 (2020)

Hameed, M.F.O., Obayya, S.S.A.: Polarization splitter based on soft glass nematic liquid crystal photonic crystal fiber. IEEE Photonics J. (2009). https://doi.org/10.1109/JPHOT.2009.2037977

Hameed, M.F.O., Obayya, S.S.A.: Analysis of polarization rotator based on nematic liquid crystal photonic crystal fiber. J. Light. Technol. **28**, 806–815 (2010)

Hameed, M.F.O., Obayya, S.S.A., El-Mikati, H.A.: Highly nonlinear birefringent soft glass photonic crystal fiber with liquid crystal core. IEEE Photonics Technol. Lett. **23**, 1478–1480 (2011a)

Hameed, M.F.O., Obayya, S.S.A., El-Mikati, H.A.: Passive polarization converters based on photonic crystal fiber with L-shaped core region. J. Light. Technol. **30**, 283–289 (2011b)

Hameed, M.F.O., Alrayk, Y.K.A., Shaalan, A.A., El Deeb, W.S., Obayya, S.S.A.: Design of highly sensitive multichannel bimetallic photonic crystal fiber biosensor. J. Nanophotonics **10**, 46016 (2016)

Heidari, M., Faramarzi, V., Sharifi, Z., Hashemi, M., Bahadori-Haghighi, S., Janjan, B., Abbott, D.: A high-performance TE modulator/TM-pass polarizer using selective mode shaping in a VO_2-based side-polished fiber. Nanophotonics **10**, 3451–3463 (2021). https://doi.org/10.1515/nanoph-2021-0225

Hossain, S., Shah, S., Faisal, M.: Ultra-high birefringent, highly nonlinear $Ge_{20}Sb_{15}Se_{65}$ chalcogenide glass photonic crystal fiber with zero dispersion wavelength for mid-infrared applications. Optik (Stuttg) **225**, 165753 (2021)

Huang, Y., Wang, Y., Zhang, L., Shao, Y., Zhang, F., Liao, C., Wang, Y.: Tunable electro-optical modulator based on a photonic crystal fiber selectively filled with liquid crystal. J. Light. Technol. **37**, 1903–1908 (2019)

Hui, Z., Zhang, Y., Soliman, A.-H.: Mid-infrared dual-rhombic air hole Ge20Sb15Se65 chalcogenide photonic crystal fiber with high birefringence and high nonlinearity. Ceram. Int. **44**, 10383–10392 (2018)

Jeyaselvan, V., Pal, A., Kumar, P.S.A., Selvaraja, S.K.: Thermally-induced optical modulation in a vanadium dioxide-on-silicon waveguide. OSA Contin. **3**, 132–142 (2020)

Koshiba, M., Tsuji, Y.: Curvilinear hybrid edge/nodal elements with triangular shape for guided-wave problems. J. Light. Technol. **18**, 737–743 (2000)

Kumari, B., Varshney, R.K., Pal, B.P.: Design of a silicon-on-calcium-fluoride-based compact and efficient polarization rotator for the mid-IR. OSA Contin. **1**, 1158–1171 (2018)

Kumari, B., Varshney, R.K., Pal, B.P.: Design of a silicon-on-calcium-fluoride-based ultracompact and highly efficient polarization splitter for the midinfrared. Opt. Eng. **58**, 37102 (2019)

Lavchiev, V.M., Jakoby, B.: Photonics in the mid-infrared: challenges in single-chip integration and absorption sensing. IEEE J. Sel. Top. Quantum Electron. **23**, 452–463 (2016)

Liu, A., Jones, R., Liao, L., Samara-Rubio, D., Rubin, D., Cohen, O., Nicolaescu, R., Paniccia, M.: A high-speed silicon optical modulator based on a metal–oxide–semiconductor capacitor. Nature **427**, 615–618 (2004)

Liu, Z., Mei, B., Song, J., Li, W.: Optical characterizations of hot-pressed erbium-doped calcium fluoride transparent ceramic. J. Am. Ceram. Soc. **97**, 2506–2510 (2014)

Lumerical Software Package. https://www.lumerical.com/

Luzhansky, E., Choa, F.-S., Merritt, S., Yu, A., Krainak, M.: Mid-IR free-space optical communication with quantum cascade lasers. In: Laser Radar Technology and Applications XX; and Atmospheric Propagation XII. pp. 267–273. SPIE (2015)

Lyeo, H.-K., Cahill, D.G., Lee, B.-S., Abelson, J.R., Kwon, M.-H., Kim, K.-B., Bishop, S.G., Cheong, B.: Thermal conductivity of phase-change material $Ge_2Sb_2Te_5$. Appl. Phys. Lett. **89**, 151904 (2006)

Malitson, I.H.: A redetermination of some optical properties of calcium fluoride. Appl. Opt. **2**, 1103–1107 (1963)

Montesinos-Ballester, M., Deniel, L., Koompai, N., Nguyen, T.H.N., Frigerio, J., Ballabio, A., Falcone, V., Le Roux, X., Alonso-Ramos, C., Vivien, L.: Mid-infrared integrated electro-optic modulator operating up to 225 MHz between 6.4 and 10.7 μm wavelength. ACS Photonics **9**, 249–255 (2022)

Obayya, S.S.A., Rahman, B.M.A., Grattan, K.T.V., El-Mikati, H.A.: Full vectorial finite-element-based imaginary distance beam propagation solution of complex modes in optical waveguides. J. Light. Technol. **20**, 1054 (2002)
Oskooi, A.F., Roundy, D., Ibanescu, M., Bermel, P., Joannopoulos, J.D., Johnson, S.G.: MEEP: a flexible free-software package for electromagnetic simulations by the FDTD method. Comput. Phys. Commun. **181**, 687–702 (2010)
Peng, C., Ou, K., Li, G., Li, X., Wang, W., Zhao, Z., Chen, X., Lu, W.: Tunable phase change polaritonic perfect absorber in the mid-infrared region. Opt. Express. **28**, 11721–11729 (2020)
Rajarajan, M., Obayya, S.S.A., Rahman, B.M.A., Grattan, K.T.V., El-Mikati, H.A.: Design of compact optical bends with a trench by use of finite-element and beam-propagation methods. Appl. Opt. **39**, 4946–4953 (2000)
Sadeghi, M., Janjan, B., Heidari, M., Abbott, D.: Mid-infrared hybrid Si/VO_2 modulator electrically driven by graphene electrodes. Opt. Express **28**, 9198–9207 (2020)
Shadmani, A., Miri, M., Pouyan, S.M.: Ultra-wideband multi-level optical modulation in a $Ge_2Sb_2Te_5$-based waveguide with low power consumption and small footprint. Opt. Commun. **439**, 53–60 (2019)
Shadmani, A., Miri, M.: Design and simulation of dual polarization GST-on-silicon nitride optical modulator. In: 2019 27th Iranian Conference on Electrical Engineering (ICEE). pp. 220–223. IEEE (2019)
Sopko, I.M., Ignatyeva, D.O., Knyazev, G.A., Belotelov, V.I.: Efficient acousto-optical light modulation at the mid-infrared spectral range by planar semiconductor structures supporting guided modes. Phys. Rev. Appl. **13**, 34076 (2020)
Soref, R.: Mid-infrared photonics in silicon and germanium. Nat. Photonics **4**, 495–497 (2010)
Su, Y., Wang, W., Hu, X., Hu, H., Huang, X., Wang, Y., Si, J., Xie, X., Han, B., Feng, H.: 10 Gbps DPSK transmission over free-space link in the mid-infrared. Opt. Express **26**, 34515–34528 (2018)
Suda, K., Uno, T., Miyakawa, T., Sawamoto, N., Machida, H., Ishikawa, M., Sudoh, H., Ohshita, Y., Ogura, A.: $Ge_2Sb_2Te_5$ film fabrication by tellurization of chemical vapor deposited GeSb. Jpn. J. Appl. Phys. (2013). https://doi.org/10.7567/JJAP.52.128006
Tian, X., Xu, J., Xu, K., Ma, X., Duan, X., Yang, P., Ding, P., Li, Z.-Y.: Wavelength-selective, tunable and switchable plasmonic perfect absorbers based on phase change materials $Ge_2Sb_2Te_5$. Europhys. Lett. **128**, 67001 (2020)
Vassalini, I., Alessandri, I., de Ceglia, D.: Stimuli-responsive phase change materials: optical and optoelectronic applications. Materials (Basel) **14**, 3396 (2021)
Wang, F., Chen, Y., Ma, T., Liu, H., Wang, X., Jin, C.: Mid-infrared polarization rotator based on a Si_3N_4–CaF_2 hybrid plasmonic waveguide with asymmetric metal claddings. Appl. Opt. **60**, 2441–2449 (2021)
Wang, F., Chen, Y., Li, C., Ma, T., Wang, X., Yu, K., Li, L.: Ultracompact and broadband mid-infrared polarization beam splitter based on an asymmetric directional coupler consisting of GaAs–CaF_2 hybrid plasmonic waveguide and GaAs nanowire. Opt. Commun. **502**, 127418 (2022)
Wen, C., Banshchikov, A.G., Illarionov, Y.Y., Frammelsberger, W., Knobloch, T., Hui, F., Sokolov, N.S., Grasser, T., Lanza, M.: Dielectric properties of ultrathin CaF_2 ionic crystals. Adv. Mater. **32**, 2002525 (2020)
Wu, Z., Chen, Y., Zhang, T., Shao, Z., Wen, Y., Xu, P., Zhang, Y., Yu, S.: Design and optimization of optical modulators based on graphene-on-silicon nitride microring resonators. J. Opt. **19**, 45801 (2017)
Xie, Q., Chen, Y., Li, X., Yin, Z., Wang, L., Geng, Y., Hong, X.: Characteristics of D-shaped photonic crystal fiber surface plasmon resonance sensors with different side-polished lengths. Appl. Opt. **56**, 1550 (2017). https://doi.org/10.1364/ao.56.001550
Yamada, K., Tsuchizawa, T., Nishi, H., Kou, R., Hiraki, T., Takeda, K., Fukuda, H., Ishikawa, Y., Wada, K., Yamamoto, T.: High-performance silicon photonics technology for telecommunications applications. Sci. Technol. Adv. Mater. (2014). https://doi.org/10.1088/1468-6996/15/2/024603
Zhang, L., Agarwal, A.M., Kimerling, L.C., Michel, J.: Nonlinear Group IV photonics based on silicon and germanium: from near-infrared to mid-infrared. Nanophotonics **3**, 247–268 (2014)
Zheng, G.-M.: Mid-infrared broadband polarization beam splitter based on GaS photonic crystal fiber with high extinction ratio. Optik (Stuttg) **241**, 166971 (2021)
Zhou, Y., Chen, X., Ko, C., Yang, Z., Mouli, C., Ramanathan, S.: Voltage-triggered ultrafast phase transition in vanadium dioxide switches. IEEE Electron Device Lett. **34**, 220–222 (2013)
Zhou, W.B., Cai, F.F., Zhi, G.L., Mei, B.C.: Fabrication of highly-transparent Er: CaF_2 ceramics by hot-pressing technique. Mater. Sci. **32**, 358–363 (2014)